

# Characterizing the Bulk-Boundary Correspondence of one-dimensional non-Hermitian interacting systems by edge entanglement entropy

Weitao Chen,<sup>1</sup> Liangtao Peng,<sup>1</sup> Hantao Lu,<sup>2,\*</sup> and Xiancong Lu<sup>1,†</sup>

<sup>1</sup>*Department of Physics, Xiamen University, Xiamen 361005, China*

<sup>2</sup>*School of Physical Science and Technology & Key Laboratory for Magnetism and Magnetic Materials of the MoE, Lanzhou University, Lanzhou 730000, China*

(Dated: February 16, 2022)

Dramatically different from the Hermitian systems, the conventional Bulk-Boundary Correspondence (BBC) is broken in the non-Hermitian systems. In this article, we use edge entanglement entropy to characterize the topological properties of non-Hermitian Su-Schrieffer-Heeger Hubbard model. For free Fermions, we study the scaling behavior of entanglement entropy and demonstrate that the edge entanglement entropy is a good indicator to delimit different phases of non-Hermitian systems. We further generalize the edge entanglement entropy to the non-Hermitian interacting Hubbard chain, and obtain the topological phase diagram in the plane of interaction and non-Hermitian hopping amplitudes. It is found that the Hubbard interaction diminishes and weakens the breakdown of Bulk-Boundary Correspondence, which eventually disappears at some critical value of interaction.

PACS numbers: PACS

## I. INTRODUCTION

Fascinating phenomena emerge in non-Hermitian systems with gain and loss of energy [1–16], which attract considerable attention from many fields of physics [17]. Various non-Hermitian systems have been intensively investigated in recent years, such as acoustics [18, 19], optics [20–22], ultra-cold atoms [23–27], parity-time-symmetric systems [28–30], driven-dissipative systems [31–35], and material junctions [36–40]. From the theoretical point of view, significant progress has been made on understanding the topological properties of non-Hermitian systems, by generalizing the conceptions from Hermitian topological band theory [41, 42]. Especially, the bulk-boundary correspondence (BBC), which states that topological invariants computed from the Bloch Hamiltonian under periodic boundary condition (PBC) exactly correspond to the boundary states under open boundary condition (OBC) [43–45], is a general principle of topological theory for Hermitian systems. However, it is shown that the BBC is broken in the non-Hermitian system [46–49], due to the sensitivity of energy spectrum to the boundary conditions. The mechanism of the breakdown of BBC has been studied [48–55] and methods to reconstruct the BBC have been proposed, *e.g.*, the generalized Brillouin zone (GBZ) [48, 51, 52, 56–59], biorthogonal polarization [49], and singular value decomposition [60].

The non-Hermitian systems on many-body basis show different behaviors comparing with that on single-particle level. For example, the well-established non-Hermitian skin effect [48] does not appear within the many-body framework, due to the Pauli exclusion principle [61, 62]. For interacting many-body systems, quite a lot of novel

non-Hermitian phenomena have been revealed, such as the many-body localization [63], the erosion of real-space Fermi surface [61], non-Hermitian topological Mott phases in both bosonic and fermionic superlattices [64–66], the emergence of pseudospectrum in correlated Hermitian systems [67, 68], the classification of topological phases in one and zero dimension [69, 70], off-diagonal long-range order with attractive interaction [71], and skin clusters from strong interactions [72].

As far as the many-body physics is concerned, quantum entanglement provides a unique perspective and has been proved to be a powerful tool to understand the phases of Hermitian systems [73–75]. For instance, the entanglement entropy (EE) was employed to identify topological orders in long-range entangled systems like quantum spin liquid [76–80]. For the one-dimensional (1D) gapped systems, the entanglement entropy of ground state obeys the well-known area-law [81–83], whereas it exhibits logarithmic scaling behavior for a gapless critical chain, with the emergence of conformal field theory (CFT) [84–86]. A natural question is what is the entanglement properties of non-Hermitian systems. Recently, this topic receives significant progress, *e.g.*, the conception of EE has been successfully extended to the non-Hermitian many-body systems [61, 62, 86–94]. In particular, the scaling behavior of EE at critical points as well as the normal phases have been well studied for various non-Hermitian non-interacting models [61, 86, 88, 93–95]. In spite of these works on free Fermions, the entanglement properties of interacting non-Hermitian systems have not been fully explored yet, and how the entanglement behavior is modified by interaction as well as its relation to topology remain unclear.

In this paper, we address this issue by studying the non-Hermitian Su-Schrieffer-Heeger (SSH) model with Hubbard interaction (SSH<sub>H</sub>), using the Exact Diagonal-

\* luht@lzu.edu.cn

† xlu@xmu.edu.cn

ization (ED) method. We will specifically focus on the edge entanglement entropy, which is firstly introduced to measure edge degeneracy of topological states in Hermitian SSH model [96]. It is proposed in Ref. [62] that the edge EE is a useful tool to detect the topological properties of non-Hermitian many-body systems. However, only non-interacting Hamiltonian is tested there, and interacting non-Hermitian models have not been verified yet, which is our main starting point. We will show in this paper that the edge EE is a good indicator of the breakdown of BBC for non-Hermitian systems. Based on edge EE, we demonstrate that the breakdown of BBC is diminished as the Hubbard interaction is increasing. The paper is organized as follows: In Sec. II, we introduce the Hamiltonian of non-Hermitian model and review the methods to calculate the EE. In Sec. III, we present the results of EE in a non-interacting non-Hermitian SSH model, in which the scaling behavior and phase transitions are studied. In Sec. IV, we present the phase diagram for interacting non-Hermitian model, according to the edge entanglement entropy. A brief summary is given in Sec. V.

## II. MODEL AND ENTANGLEMENT ENTROPY

We consider the 1D spinful non-Hermitian version of SSH model, described by the following Hamiltonian

$$H = - \sum_{i,\sigma} \left\{ [t - (-1)^i \delta t] c_{i\sigma}^\dagger c_{i+1,\sigma} + H.c. \right\} + \gamma \sum_{i,\sigma} (c_{i\sigma}^\dagger c_{i+1,\sigma} - c_{i+1,\sigma}^\dagger c_{i\sigma}) + U \sum_i n_{i\uparrow} n_{i\downarrow} \quad (1)$$

where  $c_{i\sigma}^\dagger$  ( $c_{i\sigma}$ ) is the fermionic creation (annihilation) operator at the  $i$ -th site with spin  $\sigma$  ( $\sigma = \uparrow, \downarrow$ ),  $t_1 = -(t + \delta t)$  and  $t_2 = -(t - \delta t)$  are the hopping amplitudes inside and between unit cells,  $\gamma$  denotes the non-reciprocal contribution to the hopping,  $n_{i\sigma} = c_{i\sigma}^\dagger c_{i\sigma}$  is particle number, and  $U$  is the on-site Hubbard interaction. In the remainder of this paper, we set  $t$  as the energy unit of the system, *i.e.*,  $t = 1$ . The second term in Hamiltonian (1) with  $\gamma \neq 0$  is the source of non-Hermiticity, in which the part hopping to the left is different from that hopping to the right (its Hermitian conjugate) leading to the directional localization of bulk states. This model, with a schematic figure shown in Fig. 1(a), can be experimentally realizable in an ultracold fermionic system with atom loss [25–27]. The interaction can be easily tuned through Feshbach resonances, the hopping amplitude is controlled by the depth of optical lattices, while the non-reciprocal term can be realized by laser-induced atom loss [25, 97].

To investigate the non-Hermitian model (1), we use the biorthogonal formulation of quantum mechanics [98]. For a diagonalizable non-Hermitian Hamiltonian  $H$ , one have

$$H |\Phi_{R,n}\rangle = E_n |\Phi_{R,n}\rangle, \quad H^\dagger |\Phi_{L,n}\rangle = E_n^* |\Phi_{L,n}\rangle. \quad (2)$$

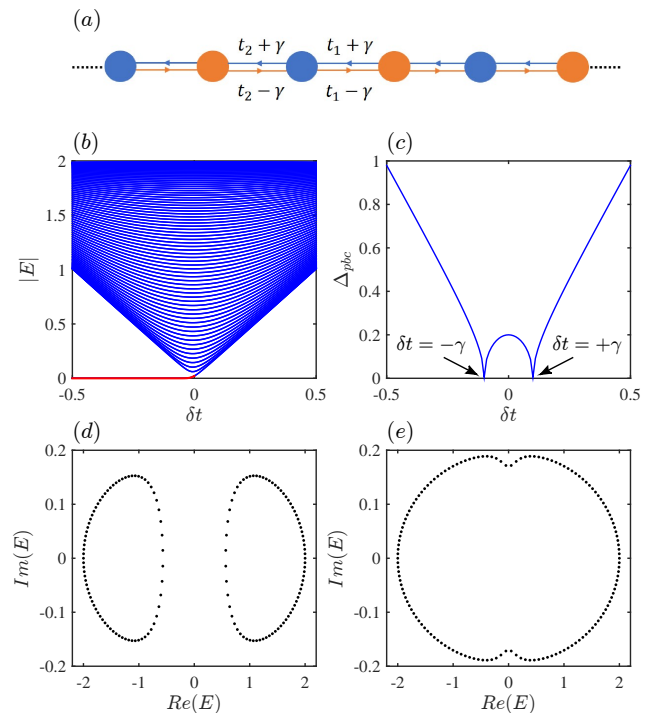


FIG. 1. (a) Schematic picture for the non-Hermitian SSH model (1). (b) The energy spectrum  $|E|$  under OBC for the non-interacting fermions with the number of lattice sizes  $L = 150$ . The red line denotes the zero modes. (c) The gap  $\Delta_{pbc}$  extracted from the absolute values of Bloch band with PBC. Two types of energy spectrum under PBC, showing the line gap (d) and point gap (e) with  $\delta t = -0.3$  and  $\delta t = -0.05$ , respectively. The values of other parameters are  $U = 0$  and  $\gamma = 0.1$ .

Here  $|\Phi_{L,n}\rangle$  and  $|\Phi_{R,n}\rangle$  are left and right eigenvectors, which can be chosen to satisfy the biorthonormality condition  $\langle \Phi_{L,m} | \Phi_{R,n} \rangle = \delta_{mn}$ . The biorthonormal expectation value of an observable  $\hat{A}$  can be computed using both left and right states of a system,  $\langle \hat{A} \rangle = \langle \Psi_L | \hat{A} | \Psi_R \rangle$ , in which any right state  $|\Psi_R\rangle$  can be decomposed into the eigenstates  $|\Psi_R\rangle = \sum_n C_n |\Phi_{R,n}\rangle$  and the corresponding left state is defined as  $|\Psi_L\rangle = \sum_n C_n |\Phi_{L,n}\rangle$  such that  $\langle \Psi_L | \Psi_R \rangle = 1$  [62, 88]. For non-Hermitian systems with complex energy  $E_n$ , there is no longer a natural way to define the many-body ground state, and different schemes of definition have been adopted before [86, 88, 93]. In this paper, we choose the left and right many-body ground states to be the ones that have the lowest real part energy, *i.e.*, by filling up the levels to Fermi energy according to the real part of the energy, as has been used in Refs. [62, 86, 88, 93].

Entanglement is one of the most fundamental properties of many-body quantum state, which is measured by EE, a quantity built from density matrix. Based on the biorthogonal formulation, the density matrix of non-Hermitian system is defined as  $\rho^{RL} = |\Psi_R\rangle \langle \Psi_L|$ , which in general is non-Hermitian ( $\rho^{RL})^\dagger \neq \rho^{RL}$ . Note that an-

other type of density matrix is given by  $\rho^{RR} = |\Psi_R\rangle\langle\Psi_R|$ , which also contains information of the system [88, 92] but is not studied in this paper. By partitioning the total system into two subsystems  $A$  and  $B$ , and then taking the partial trace over the subsystem  $B$ , the reduced density matrix of subsystem  $A$  can be calculated  $\rho_A^{RL} = Tr_B \rho^{RL}$ . The entanglement entropy is the von-Neumann entropy of non-Hermitian reduced density matrix,

$$S \equiv -Tr(\rho_A^{RL} \ln \rho_A^{RL}), \quad (3)$$

which is a straightforward generalization of the definition for Hermitian system [62, 86, 88]. Note that the non-Hermitian entanglement entropy given in Eq. (3) can be negative or complex [86, 88, 94, 95], due to the possible negative or complex eigenvalues of  $\rho_A^{RL}$ . This challenges the probability interpretation of the eigenvalues of density matrix [94]. The higher order ( $\alpha$  order) entanglement entropy, Renyi entanglement entropy, for non-Hermitian systems is defined as

$$S_\alpha \equiv \frac{1}{1-\alpha} \ln Tr[(\rho_A^{RL})^\alpha]. \quad (4)$$

The von-Neumann entanglement entropy can be obtained from Renyi entropy by letting  $\alpha \rightarrow 1$ :  $S \equiv S_1 = \lim_{\alpha \rightarrow 1} S_\alpha$ . Based on the Renyi entanglement entropy, the edge entanglement entropy is given by [62, 96]

$$S_{\alpha,edge} \equiv S_{\alpha,OBC} - \frac{1}{2}S_{\alpha,PBC}, \quad (5)$$

where  $S_{\alpha,OBC}$  and  $S_{\alpha,PBC}$  are calculated under OBC and PBC, respectively. Due to the area law that entanglement entropy obeys, the difference between  $S_{\alpha,OBC}$  and half of  $S_{\alpha,PBC}$  contains the topological information of edge states such as the degeneracy [96]. Especially for the Hermitian SSH model, the  $S_{2,edge}$  exhibits a quantized value  $2 \ln 2$  (0) in the gapped topological (trivial) phase [43, 96]. For the non-Hermitian non-interacting SSH model, a similar quantized behavior was observed [62], but only in a specific regions as will be shown in the next section.

For the free Fermions, the correlation matrix is an efficient technique to compute the reduced density matrix and the entanglement entropy [99–101]. It is shown that, within the framework of biorthogonal formulation, the method of correlated matrix is also valid for the non-interacting non-Hermitian system [86, 88]. The key procedure is to write the reduced density matrix as  $\rho_A^{RL} = \frac{1}{Z} \exp(-\tilde{H})$ , with  $\tilde{H} = \sum_{\alpha\beta} h_{\alpha\beta} c_\alpha^\dagger c_\beta$  being the entanglement Hamiltonian. The Hamiltonian matrix  $\mathbf{h}$  can be written in terms of the two-site correlation matrix  $\mathbf{C}^A$  [86, 88], *i.e.*,  $\mathbf{h} = \ln[(1 - \mathbf{C}^A)/\mathbf{C}^A]$ , where the elements of  $\mathbf{C}^A$  are restricted to the subsystem  $A$  and are defined as  $C_{ij}^A = \langle \Psi_L | c_i^\dagger c_j | \Psi_R \rangle = Tr(\rho_A^{RL} c_i^\dagger c_j)$ . Once the eigenvalues  $\xi_i$  of matrix  $\mathbf{C}^A$  is known by diagonalization, the entanglement spectrum of  $\rho_A^{RL}$  is given by  $\epsilon_i = \ln[(1 - \xi_i)/\xi_i]$ , and thus the entanglement entropy

as well

$$S = - \sum_l \left[ \xi_l \ln \xi_l + (1 - \xi_l) \ln(1 - \xi_l) \right] \quad (6)$$

$$S_\alpha = \frac{1}{1-\alpha} \sum_l \ln \left[ (1 - \xi_l)^\alpha + \xi_l^\alpha \right]. \quad (7)$$

For the interacting non-Hermitian system, the method of correlated matrix is no longer valid. We then turn to the non-Hermitian Lanczos ED method [102] to compute the entanglement entropy. In practice, the ED method begins with representing the many-body basis in Hilbert space. For the model in Eq. (1), a convenient basis can be constructed in real space as  $|\psi\rangle = \prod_{i=1}^L (c_{i\uparrow}^\dagger)^{n_i^\uparrow} \prod_{j=1}^L (c_{j\downarrow}^\dagger)^{n_j^\downarrow} |0\rangle$ , where  $n_i^\sigma \in \{0, 1\}$  indicates whether or not site  $i$  is occupied by a spin- $\sigma$  electron. A sequence of values  $\{n_i^\sigma\}$  can be interpreted as a bit-pattern, which uniquely corresponds to an integer  $I^\sigma$ . In this way, each basis-state is represented by a pair of integers ( $I^\uparrow, I^\downarrow$ ) [103, 104]. After generating the basis states in order, the elements of Hamiltonian matrix can be computed by suitable bit-level operations [104]. The Hamiltonian matrix is sparse in this representation, and only nonzero elements are stored to save memory and speed up operations. The following key step is to diagonalize the Hamiltonian matrix using non-Hermitian Lanczos method, which is a two-sided iterative algorithm [102]. By using the relation of recurrence, two sequences of Lanczos vectors can be generated, which are biorthogonal and span the left and right Krylov spaces. The Hamiltonian matrix in these Lanczos bases is a non-Hermitian tridiagonal matrix whose eigenvectors can be used to construct the eigenvectors of the original Hamiltonian [102–104]. The right (left) ground state vector obtained from Lanczos can be projected onto a right (left) tensor with a rank  $L$ , the number of total lattice sites. After cutting the system, the right (left) tensor can be further reshaped into a  $4^{L_A}$ -by- $4^{L_B}$  right (left) matrix  $T_R$  ( $T_L$ ), where  $L_A$  and  $L_B$  are the lattice sizes of subsystems  $A$  and  $B$ , respectively. The matrix  $T_R$  ( $T_L$ ) corresponds to a direct product of the right (left) eigenvectors of  $A$  and  $B$ . The partial trace over  $B$  can be easily performed by matrix multiplication and the reduced density matrix can be calculated by  $\rho_A^{RL} = T_R^\dagger T_L$ . With  $\rho_A^{RL}$ , the entanglement entropy can be worked out through their definitions in Eqs. (3) and (4).

### III. NON-HERMITIAN FREE-FERMIONIC SSH MODEL

We firstly focus on the non-interacting system with  $U = 0$ . In this case, the non-Hermitian SSH model shows the breakdown of conventional BBC [46–49], *i.e.*, the topological transition points extracted from the edge states of OBC differ from the gap-closing points of the Bloch Hamiltonian under PBC. For the model in Eq. (1), the topological transition point locates at  $\delta t = 0$ , whereas

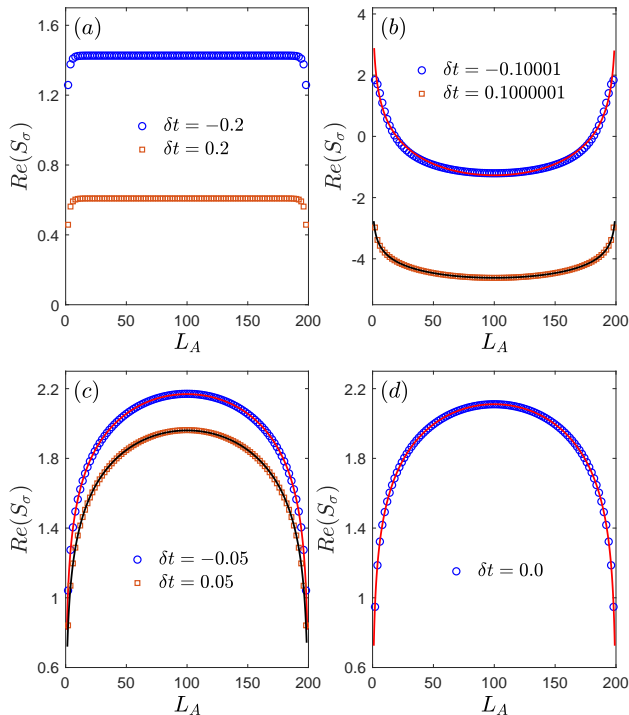


FIG. 2. The scaling behavior of the real part of von-Neumann entanglement entropy  $S_\sigma$  for one spin component ( $\sigma = \uparrow, \downarrow$ ) of non-Hermitian free fermions. The system is under PBC and at half-filling. The values of hopping dimerization  $\delta t$  in each sub-figure are: (a)  $\delta t = -0.2$  and  $0.2$ ; (b)  $\delta t = -0.10001$  and  $0.1000001$ ; (c)  $\delta t = -0.05$  and  $0.05$ ; (d)  $\delta t = 0.0$ . The values of other parameters are  $U = 0$ ,  $\gamma = 0.1$ , and total lattice sizes  $L = 200$ . The solid lines in sub-figures (b), (c) and (d) are the fitting curves using Eq. (8) with  $\alpha = 1$ .

the gap-closing points are at  $\delta t = \pm\gamma$ , as shown in Fig. 1(b) and (c) where the energy spectrum of OBC and absolute gap of PBC are plotted. These three transition points delimit four different phases in the whole parameter region. Moreover, two types of gaps can be observed: the point gap within  $-\gamma < \delta t < \gamma$  and the line gap when  $\delta t > \gamma$  and  $\delta t < -\gamma$ ; see Fig. 1(d) and (e) for typical examples. The type of gap will greatly influence the topological properties of the Hamiltonian [50, 88, 105].

The real part of von-Neumann entanglement entropy under PBC is plotted in Fig. 2 against the subsystem size  $L_A$ , with a fixed total lattice size  $L = 200$ . To study the critical behavior, we fit the entanglement entropy using the following universal formula [75, 106]

$$S_\alpha(L_A) = \frac{c}{6} \left(1 + \frac{1}{\alpha}\right) \ln \left( \frac{L}{\pi} \sin \left[ \frac{\pi L_A}{L} \right] \right) + s_\alpha + \dots \quad (8)$$

where  $c$  is the central charge described by conformal field theory (CFT),  $s_\alpha$  is a non-universal constant term, and  $\alpha$  is the order of Renyi entropy which is chosen to be  $\alpha = 1$  for the case of von-Neumann entropy. As will be shown below, the non-Hermitian entanglement entropy exhibits scaling behavior of Eq. (8) around the critical points as

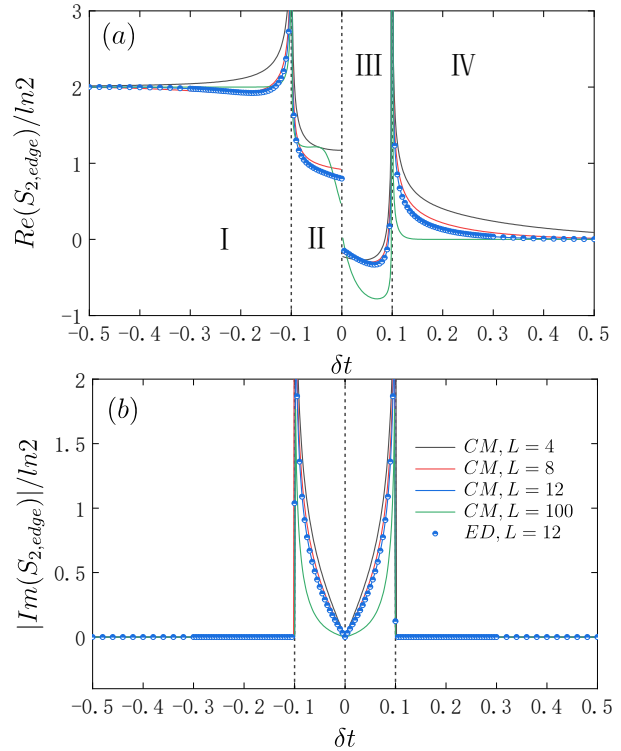


FIG. 3. The second order edge entanglement entropy  $S_{2,edge}$ , calculated by the correlation matrix (CM) method (lines, with  $L = 4, 8, 12$ , and  $100$ ) and ED method (blue circle,  $L = 12$ ), as a function of the hopping dimerization  $\delta t$ . The system is at half-filling with  $N_\uparrow = N_\downarrow = L/2$ ,  $U = 0$ , and  $\gamma = 0.1$ . Four phases, from I to IV, can be discriminated by using two gap-closing points at  $\delta t = \pm\gamma$  and one critical point at  $\delta t = 0$ .

well as in the point gap phases.

In the regions  $\delta t > \gamma$  and  $\delta t < -\gamma$ , the von-Neumann EE is always real and gets saturated to a constant value as the increase of subsystem size  $L_A$ , implying that the system is non-critical and is short-range correlated; See Fig. 2(a) for typical examples. This behavior is related to the gap structure of energy band, *i.e.*, the real line gap as shown in Fig. 1(d). In this case, non-Hermitian Hamiltonian may be continuously deformed into a Hermitian Hamiltonian without breaking of symmetries [88]. At  $\delta t = \pm\gamma$ , the line gap transforms into the point gap (gap-closing points), and therefore a PBC phase transition occurs. The real part of von-Neumann EE, shown in Fig. 2(b), displays a logarithmic dependence on the subsystem size  $L_A$ , when shifting away from the critical points  $\delta t = \pm 0.1$  by a tiny value  $\epsilon$  [86, 94, 95]. By fitting the data using Eq. (8), we obtain  $c = -1.3367$ ,  $s_1 = -2.7697$  for  $\delta t = 0.1000001$  ( $\epsilon = 1 \times 10^{-7}$ ), while  $c = -3.2026$ ,  $s_1 = 3.1642$  for  $\delta t = -0.10001$  ( $\epsilon = 1 \times 10^{-5}$ ). The values of  $c$  and  $s_1$  strongly depend on the way one approaching the critical points from the line-gap side [86, 94], *e.g.*, the magnitude of shift  $\epsilon$ . For the critical point

$\delta t = 0.1$ , the absolute value  $|c|$  seems to converge to a value around 1.34 when  $\epsilon \rightarrow 0$ . However, for the critical point  $\delta t = -0.1$ , the value  $|c|$  increases as  $\epsilon \rightarrow 0$  and a violation of the universal relation in Eq. (8) is observed after  $\epsilon < 1 \times 10^{-5}$ . When entering the region  $-\gamma < \delta t < \gamma$ , the scaling of real part of EE crosses over from a concave ( $c < 0$ ) to convex ( $c > 0$ ) function [86]; See Fig. 2(c) for examples, in which  $c = 0.9767$ ,  $s_1 = 0.8164$  and  $c = 0.9748$ ,  $s_1 = 0.6105$  are obtained for  $\delta t = -0.05$  and  $\delta t = 0.05$ , respectively. It is interesting that the whole region of  $-\gamma < \delta t < \gamma$  is critical with long-range correlations [88]. The point  $\delta t = 0$  is a topological critical point, at which the EE is real and the fitting central charge is  $c = 1.0007$  with  $s_1 = 0.7252$ .

The edge entanglement entropy defined in Eq.(5) is a useful tool to detect the topological properties of both noninteracting and interacting many-body systems [62, 96, 107, 108]. It measures the entanglement between two edges of a finite chain and converges to edge degeneracy in the thermodynamic limit [96, 109]. In Fig. 3, the second-order edge entanglement entropy  $S_{2,edge}$  of non-interacting SSH model is plotted as a function of  $\delta t$  for a fixed value of  $\gamma = 0.1$ . We use the same scheme as Ref. [96] to cut the system: When  $\delta t > 0$ , the subsystem  $A$  are chosen as  $[1; L/2]$  for both PBC and OBC chains; When  $\delta t < 0$ , subsystem  $A$  are chosen as  $[1; L/2 + 1]$  for OBC chain, but as  $[2; L/2 + 1]$  for PBC chain. By this way, all the cuts are at the weak bonds [96].

Again, four phase are recognized in Fig. 3: the line-gap topological phase (phase *I*,  $\delta t < -\gamma$ ), point-gap topological phase (phase *II*,  $-\gamma < \delta t < 0$ ), point-gap trivial phase (phase *III*,  $0 < \delta t < \gamma$ ), and line-gap trivial phase (phase *IV*,  $\delta t > \gamma$ ). In phases *I* and *IV*, the values of  $S_{2,edge}$  are real and are quantized to  $2 \ln 2$  and 0, respectively. Therefore, there are two degenerated edge modes in phase *I* and no edge modes in phase *IV* [62], the same as the topological and trivial phases of Hermitian SSH model [96]. In phases *II* and *III*, the values of  $S_{2,edge}$  are complex and are no longer quantized. The imaginary part of  $S_{2,edge}$  is rooted in the point-gap structure of energy spectrum, an unique character of non-Hermitian systems. The value of  $S_{2,edge}$  is divergent as expected at the phase-transition points  $\delta t = \pm\gamma$  (gap-closing points), while shows a jump at topological critical point  $\delta t = 0$ . In the topological phase, the edge states appear under OBC (also see Fig. 5), which will contribute a finite value to  $S_{2,edge}$  and cause the jump. As the lattice size  $L$  increases, the peaks of  $S_{2,edge}$  around critical points  $\delta t = \pm 0.1$  are narrowed, and the jump at critical point  $\delta t = 0$  becomes smaller. Note that this jump should decrease to zero in the thermodynamic limit  $L \rightarrow \infty$  for there is no difference between OBC and PBC any longer. An important feature of Fig. 3 is that, even for a small lattice size (*e.g.*,  $L = 4$ ), the  $S_{2,edge}$ , which includes information from both OBC and PBC chains, gives the correct positions of three critical points. We therefore conclude that edge entanglement entropy is a good indicator to discriminate different phases of non-Hermitian

systems.

The edge entanglement entropy calculated by correlation matrix method exactly matches that obtained by Lanczos ED method when  $U = 0$ ; see an example of  $L = 12$  in Fig. 3. Note that there is a phase random in the ground-state energy of Lanczos method. Due to the time-reversal symmetry  $T_+$  [105], the energy spectra of Hamiltonian (1) is composed of complex conjugate pairs  $E_n$  and  $E_n^*$ . However, in the routines of Lanczos algorithm, the eigenvalues pairs are not exactly complex conjugate each other, *e.g.*, their real parts are tiny different. The ground state energy is chosen according to the smallest real part, so that the sign of its imaginary part is numerically "random" (+ or -). This results in the "random"  $\pm$  sign in the imaginary part of entanglement entropy. In order to compare with the correlated matrix method, we therefore plot the absolute value of imaginary part of  $S_{2,edge}$  in Fig. 3.

#### IV. NON-HERMITIAN INTERACTING SSH MODEL

We then move to study the BBC of non-Hermitian interacting SSH model, by examining the edge entanglement entropy computed using the non-Hermitian ED method described in Sec. II. The numerical results of second-order edge entanglement entropy  $S_{2,edge}$  are presented in Fig. 4 for various values of interaction  $U$ . When the  $U$  is small, the overall behavior of  $S_{2,edge}$  is similar to the noninteracting case, except for the quantized value in phase *I* which decreases from  $2 \ln 2$  to  $\ln 2$ . The Hubbard  $U$  will raise the energy of doubly occupied edge state on the right (or left) end of a open chain, and therefore reduce the edge degeneracy 4 to 2, which results in the decrease of  $S_{2,edge}$  [96]. When  $U$  is increasing as in Fig. 4(b), the critical points on two sides move towards the center at  $\delta t = 0$ , *i.e.*, the regions of non-Hermitian phases *II* and *III* are narrowed and also the imaginary parts of  $S_{2,edge}$  in them are suppressed. For very large value of  $U$  as in Fig. 4(c), three critical points merge into the one at  $\delta t = 0$ , and the non-Hermitian phases *II* and *III* disappear in the phase diagram. In this case, the system behaves like a Hermitian one with a real value of  $S_{2,edge}$ , which suggests that the effects of non-Hermiticity is killed by the interaction.

The particle density,  $|\psi_{LR}|^2 = \langle \Psi_L | \sum_{\sigma} n_{i,\sigma} | \Psi_R \rangle$ , on each sites of a interacting chain under OBC is shown in Fig. 5, for  $U = 1$  and four typical values of  $\delta t$ . At half-filling (blue dots), the distribution of particle is homogeneous over the whole lattice, no matter what values of  $\delta t$  are. To detect the edge modes, we add or remove one particle from the half-filling case [62]. The additional particle (hole) is localized near the edges when the system is in topologically non-trivial phases ( $\delta t < 0$ ) as in Fig. 5(a) and (b). The amplitude of edge mode in phase *II* [Fig. 5(b)] is much smaller than that in phase *I* due to the strong interference of non-Hermiticity, and it

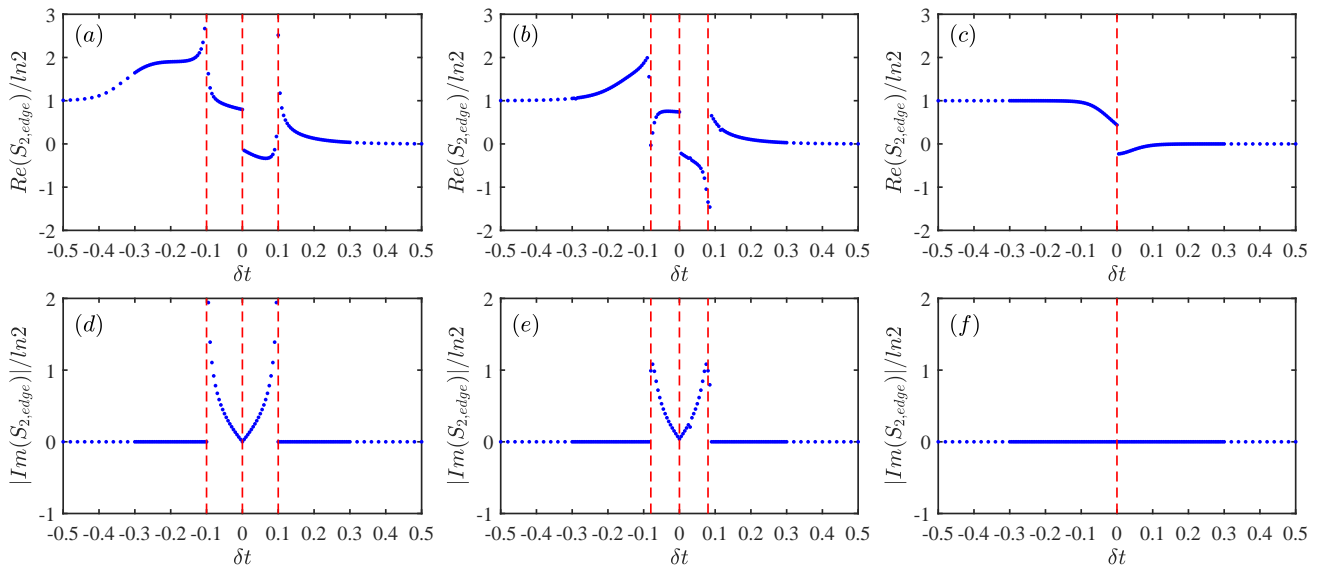


FIG. 4. The real and imaginary parts of second order edge entanglement entropy  $S_{2,edge}$  as a function of the hopping dimerization  $\delta t$  for various interaction  $U$ . For (a) and (d),  $U = 0.1$ ; for (b) and (e),  $U = 1$ ; for (c) and (f),  $U = 10$ . The system is at half-filling with  $L = 12$  and  $\gamma = 0.1$ . The cut scheme used in the calculations is the same as that in Fig. 3.

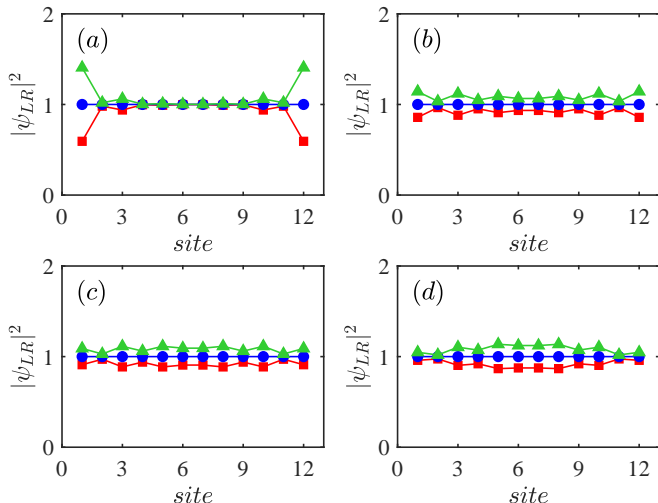


FIG. 5. The distribution of particle density  $|\psi_{LR}|^2$  of an open chain at finite interaction  $U = 1$ . The blue dots correspond to the density at half-filling, while the green upward triangles (red square) are the density by adding (removing) one particle from the half-filling case. The values of parameters are  $L = 12$  and  $\gamma = 0.1$ . From (a) to (d),  $\delta t = -0.5, -0.08, 0.08, \text{ and } 0.5$ , respectively.

will decrease to zero also when  $\delta t$  approaching zero. For the topologically trivial phases ( $\delta t > 0$ ), the additional particle (hole) always spreads over the entire lattices, as shown in Fig. 5(c) and (d), which means no edge modes in these phases.

To further reveal the details on the competition between the interaction and the non-Hermiticity, we plot the comprehensive phase diagram in Fig. 6 in the plane

of  $\delta t$  and  $U$ , according to the real and imaginary parts of second-order edge entanglement entropy  $S_{2,edge}$ . The phase diagram can still be roughly divided into four phases: the  $S_{2,edge}$  is real for phases I and IV, while the imaginary part of  $S_{2,edge}$  is nonzero for phases II and III, due to the different gap structure of energy spectrum. As the increase of  $U$ , the point-gap region, characterized by the imaginary part of  $S_{2,edge}$  (phases II and III), is narrowing and eventually disappears around  $U \approx 2.0$ , which forms a dome shape in the phase diagram. Note that the boundary of this dome is blurred and irregular, which may due to the large quantum fluctuations here. When  $U$  is large, the quantized value of  $S_{2,edge}$  is robust, *i.e.*,  $S_{2,edge}$  equals to  $\ln 2$  and 0 in phase I and phase IV, respectively; see also Fig. 4(c). There is only one topological transition point at  $\delta t = 0$ , implying that the behavior of system is similar to the Hermitian one and the BBC recovers again.

The overall behaviors of phase boundaries with different lattice size (*e.g.*,  $L = 12$  and  $L = 8$ ) are similar, although slightly differences appear in the intermediate  $U$  region (close to the critical interaction  $U_c$ ) where the quantum fluctuations are large. This implies that the finite-size effect is not severe in determining the phase boundary according to  $S_{2,edge}$ . Note that it is also difficult to compute  $S_{2,edge}$  for a system with large  $L$ , for one need to diagonalize a chain with OBC where the translational invariance can not be utilized in Lanczos method.

The disappearance of non-Hermitian phases II and III in the phase diagram can be understood from the viewpoint of Mott physics. For a system at half-filling, Hubbard  $U$  tends to localize the particles in real space and pushes the system into the Mott-insulating phase, in which the charge fluctuations (particle hopping) are

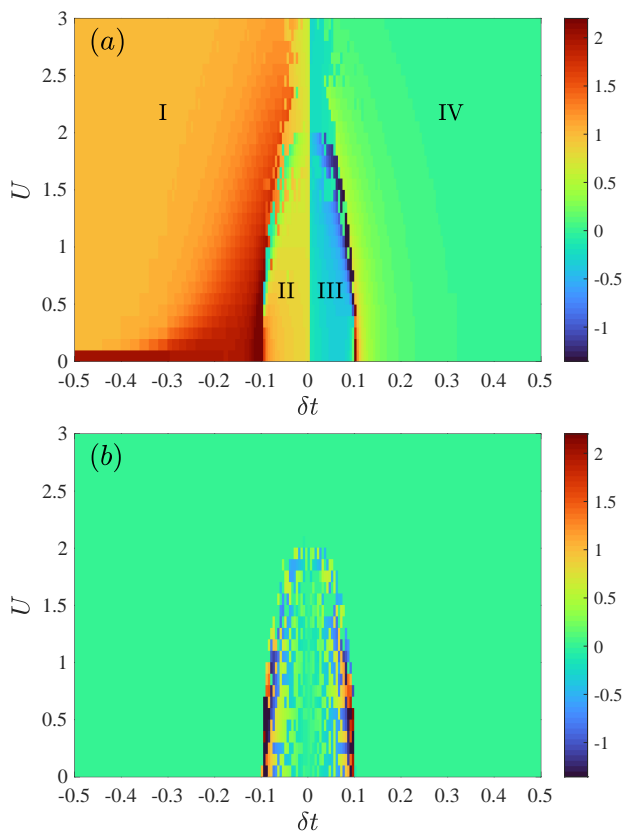


FIG. 6. The phase diagram of non-Hermitian SSH model in the plane of hopping dimerization  $\delta t$  and interaction  $U$ . The system is at half-filling with  $L = 12$  and  $\gamma = 0.1$ . Sub-figures (a) and (b) show the real and imaginary parts of second-order edge entanglement entropy  $S_{2,edge}$  (in unit of  $\ln 2$ ), respectively.

greatly suppressed. Therefore, the non-Hermitian phenomena associated with hopping term can be suppressed also when the  $U$  is increasing. Note that the physics would be significantly different if the system is away from half-filling, due to the absence of Mott phase. The destruction of non-Hermitian effects by interaction has been observed in some other works too [61, 70].

However, in another context, the interaction can result in non-Hermiticity in an original Hermitian system: the effective one-body quasiparticle Hamiltonian is non-Hermitian when the lifetimes of different type of quasiparticles are different [110–113]. The origin of non-Hermiticity in quasiparticle context is different from that in this paper (non-reciprocal hopping). It will be interesting to study the quasiparticle behavior of non-Hermitian SSH model in Eq. (1), which may exhibit novel non-Hermitian effects. We leave this topic for future study.

## V. SUMMARY

In summary, we generalize the concept of edge entanglement entropy to characterize different phases in non-Hermitian many-body systems. The effectiveness of edge entanglement entropy to detect the topological properties of non-Hermitian systems is firstly examined on the free SSH model. We demonstrated that the edge entanglement entropy, including both OBC and PBC informations, gives the correct positions of all critical points, and therefore is a good indicator for the breakdown of BBC of non-Hermitian systems. For the interacting non-Hermitian systems, we use the non-Hermitian Lanczos method to compute the entanglement entropy. A comprehensive phase diagram was obtained for the non-Hermitian SSH model, according to both real and imaginary parts of the second-order edge entanglement entropy. The interplay between non-Hermitian and Hubbard interaction is analyzed, and four different phases are identified in the phase diagram. We showed that the breakdown of BBC is diminished and weakened by the Hubbard interaction, which eventually disappears when interaction is large.

## ACKNOWLEDGMENTS

We are grateful for helpful discussions with Tian-Sheng Zeng, Hang Zhou, and Ching Hua Lee. This work is supported by the National Natural Science Foundation of China (Grant No. 11974293, No. 11874187, and No. 12174168) and the Fundamental Research Funds for Central Universities (Grant No. 20720180015).

Weitao Chen and Liangtao Peng contributed equally to this work.

- 
- [1] H. Cao and J. Wiersig, *Rev. Mod. Phys.* **87**, 61 (2015).
  - [2] K. Ding, G. Ma, M. Xiao, Z. Q. Zhang, and C. T. Chan, *Phys. Rev. X* **6**, 021007 (2016).
  - [3] K. Kawabata, Y. Ashida, and M. Ueda, *Phys. Rev. Lett.* **119**, 190401 (2017).
  - [4] M. Liertzer, L. Ge, A. Cerjan, A. D. Stone, H. E. Türeci, and S. Rotter, *Phys. Rev. Lett.* **108**, 173901 (2012).
  - [5] T. Ozawa, H. M. Price, A. Amo, N. Goldman, M. Hafezi, L. Lu, M. C. Rechtsman, D. Schuster, J. Simon, O. Zilberberg, and I. Carusotto, *Rev. Mod. Phys.* **91**, 015006 (2019).
  - [6] R. Fleury, D. Sounas, and A. Al, *Nature Communications* **6**, 5905 (2015).
  - [7] J. Doppler, A. A. Mailybaev, J. Bhm, U. Kuhl, A. Girschik, F. Libisch, T. J. Milburn, P. Rabl, N. Moiseyev, and S. Rotter, *Nature* **537**, 76 (2016).
  - [8] S. Malzard, C. Poli, and H. Schomerus, *Phys. Rev. Lett.* **115**, 200402 (2015).
  - [9] L. Chang, X. Jiang, S. Hua, C. Yang, J. Wen, L. Jiang, G. Li, G. Wang, and M. Xiao, *Nature Photonics* **8**, 524

- (2014).
- [10] H. Xu, D. Mason, L. Jiang, and J. G. E. Harris, *Nature* **537**, 80 (2016).
- [11] T. Gao, E. Estrecho, K. Y. Bliokh, T. C. H. Liew, M. D. Fraser, S. Brodbeck, M. Kamp, C. Schneider, S. Hfling, Y. Yamamoto, F. Nori, Y. S. Kivshar, A. G. Truscott, R. G. Dall, and E. A. Ostrovskaya, *Nature* **526**, 554 (2015).
- [12] K. G. Makris, R. El-Ganainy, D. N. Christodoulides, and Z. H. Musslimani, *Phys. Rev. Lett.* **100**, 103904 (2008).
- [13] A. Guo, G. J. Salamo, D. Duchesne, R. Morandotti, M. Volatier-Ravat, V. Aimez, G. A. Siviloglou, and D. N. Christodoulides, *Phys. Rev. Lett.* **103**, 093902 (2009).
- [14] C. E. Rter, K. G. Makris, R. El-Ganainy, D. N. Christodoulides, M. Segev, and D. Kip, *Nature Physics* **6**, 192 (2010).
- [15] Z. Lin, H. Ramezani, T. Eichelkraut, T. Kottos, H. Cao, and D. N. Christodoulides, *Phys. Rev. Lett.* **106**, 213901 (2011).
- [16] T. E. Lee and C.-K. Chan, *Phys. Rev. X* **4**, 041001 (2014).
- [17] Y. Ashida, Z. Gong, and M. Ueda, *Advances in Physics* **69**, 249 (2020).
- [18] G. Ma and P. Sheng, *Science advances* **2**, e1501595 (2016).
- [19] S. A. Cummer, J. Christensen, and A. Al, *Nature Reviews Materials* **1**, 16001 (2016).
- [20] F. Zangeneh-Nejad and R. Fleury, *Reviews in Physics* **4**, 100031 (2019).
- [21] R. El-Ganainy, K. G. Makris, M. Khajavikhan, Z. H. Musslimani, S. Rotter, and D. N. Christodoulides, *Nature Physics* **14**, 11 (2018).
- [22] M.-A. Miri and A. Alù, *Science* **363**, eaar7709 (2019).
- [23] A. J. Daley, *Advances in Physics* **63**, 77 (2014).
- [24] S. Kuhr, *National Science Review* **3**, 170 (2016).
- [25] J. Li, A. K. Harter, J. Liu, L. de Melo, Y. N. Joglekar, and L. Luo, *Nature Communications* **10**, 855 (2019).
- [26] S. Lapp, J. Ang'ong'a, F. A. An, and B. Gadway, *New Journal of Physics* **21**, 045006 (2019).
- [27] Z. Ren, D. Liu, E. Zhao, C. He, K. K. Pak, J. Li, and G.-B. Jo, *Topological control of quantum states in non-hermitian spin-orbit-coupled fermions* (2021), arXiv:2106.04874 [cond-mat.quant-gas].
- [28] C. M. Bender, *Reports on Progress in Physics* **70**, 947 (2007).
- [29] P. Dorey, C. Dunning, and R. Tateo, *Journal of Physics A: Mathematical and Theoretical* **40**, R205 (2007).
- [30] . K. zdemir, S. Rotter, F. Nori, and L. Yang, *Nature Materials* **18**, 783 (2019).
- [31] H. Deng, H. Haug, and Y. Yamamoto, *Rev. Mod. Phys.* **82**, 1489 (2010).
- [32] P. R. Berman, C. C. Lin, and E. Arimondo, *Advances in Atomic, Molecular, and Optical Physics* (Elsevier, 2006).
- [33] H. Ritsch, P. Domokos, F. Brennecke, and T. Esslinger, *Rev. Mod. Phys.* **85**, 553 (2013).
- [34] L. M. Sieberer, M. Buchhold, and S. Diehl, *Reports on Progress in Physics* **79**, 096001 (2016).
- [35] H. Weimer, A. Kshetrimayum, and R. Orús, *Rev. Mod. Phys.* **93**, 015008 (2021).
- [36] E. J. Bergholtz and J. C. Budich, *Phys. Rev. Research* **1**, 012003 (2019).
- [37] J. Cayao and A. M. Black-Schaffer, *Exceptional odd-frequency pairing in non-hermitian superconducting systems* (2021), arXiv:2107.04445 [cond-mat.supr-con].
- [38] P. San-Jose, J. Cayao, E. Prada, and R. Aguado, *Scientific Reports* **6**, 21427 (2016).
- [39] D. I. Pikulin and Y. V. Nazarov, *Phys. Rev. B* **87**, 235421 (2013).
- [40] D. I. Pikulin and Y. V. Nazarov, *JETP Letters* **94**, 693 (2012).
- [41] X.-L. Qi and S.-C. Zhang, *Rev. Mod. Phys.* **83**, 1057 (2011).
- [42] M. Z. Hasan and C. L. Kane, *Rev. Mod. Phys.* **82**, 3045 (2010).
- [43] S. Ryu and Y. Hatsugai, *Phys. Rev. B* **73**, 245115 (2006).
- [44] F. Grusdt, M. Höning, and M. Fleischhauer, *Phys. Rev. Lett.* **110**, 260405 (2013).
- [45] J.-W. Rhim, J. Behrends, and J. H. Bardarson, *Phys. Rev. B* **95**, 035421 (2017).
- [46] T. E. Lee, *Phys. Rev. Lett.* **116**, 133903 (2016).
- [47] Y. Xiong, *Journal of Physics Communications* **2**, 035043 (2018).
- [48] S. Yao and Z. Wang, *Phys. Rev. Lett.* **121**, 086803 (2018).
- [49] F. K. Kunst, E. Edvardsson, J. C. Budich, and E. J. Bergholtz, *Phys. Rev. Lett.* **121**, 026808 (2018).
- [50] E. J. Bergholtz, J. C. Budich, and F. K. Kunst, *Rev. Mod. Phys.* **93**, 015005 (2021).
- [51] N. Okuma, K. Kawabata, K. Shiozaki, and M. Sato, *Phys. Rev. Lett.* **124**, 086801 (2020).
- [52] K. Zhang, Z. Yang, and C. Fang, *Phys. Rev. Lett.* **125**, 126402 (2020).
- [53] D. S. Borgnia, A. J. Kruchkov, and R.-J. Slager, *Phys. Rev. Lett.* **124**, 056802 (2020).
- [54] L. Jin and Z. Song, *Phys. Rev. B* **99**, 081103 (2019).
- [55] H.-G. Zirnstein, G. Refael, and B. Rosenow, *Phys. Rev. Lett.* **126**, 216407 (2021).
- [56] K. Yokomizo and S. Murakami, *Phys. Rev. Lett.* **123**, 066404 (2019).
- [57] C. H. Lee and R. Thomale, *Phys. Rev. B* **99**, 201103 (2019).
- [58] K.-I. Imura and Y. Takane, *Phys. Rev. B* **100**, 165430 (2019).
- [59] Z. Yang, K. Zhang, C. Fang, and J. Hu, *Phys. Rev. Lett.* **125**, 226402 (2020).
- [60] L. Herviou, J. H. Bardarson, and N. Regnault, *Phys. Rev. A* **99**, 052118 (2019).
- [61] S. Mu, C. H. Lee, L. Li, and J. Gong, *Phys. Rev. B* **102**, 081115 (2020).
- [62] E. Lee, H. Lee, and B.-J. Yang, *Phys. Rev. B* **101**, 121109 (2020).
- [63] R. Hamazaki, K. Kawabata, and M. Ueda, *Phys. Rev. Lett.* **123**, 090603 (2019).
- [64] D.-W. Zhang, Y.-L. Chen, G.-Q. Zhang, L.-J. Lang, Z. Li, and S.-L. Zhu, *Phys. Rev. B* **101**, 235150 (2020).
- [65] Z. Xu and S. Chen, *Phys. Rev. B* **102**, 035153 (2020).
- [66] T. Liu, J. J. He, T. Yoshida, Z.-L. Xiang, and F. Nori, *Phys. Rev. B* **102**, 235151 (2020).
- [67] N. Okuma and M. Sato, *Phys. Rev. Lett.* **126**, 176601 (2021).
- [68] T. Yoshida, *Phys. Rev. B* **103**, 125145 (2021).
- [69] W. Xi, Z.-H. Zhang, Z.-C. Gu, and W.-Q. Chen, *Science Bulletin* **66**, 1731 (2021).



- [70] T. Yoshida and Y. Hatsugai, *Phys. Rev. B* **104**, 075106 (2021).
- [71] X. Z. Zhang and Z. Song, *Phys. Rev. B* **103**, 235153 (2021).
- [72] R. Shen and C. H. Lee, Non-hermitian skin clusters from strong interactions (2021), arXiv:2107.03414 [cond-mat.str-el].
- [73] A. Kitaev and J. Preskill, *Phys. Rev. Lett.* **96**, 110404 (2006).
- [74] M. Levin and X.-G. Wen, *Phys. Rev. Lett.* **96**, 110405 (2006).
- [75] N. Laflorencie, *Physics Reports* **646**, 1 (2016).
- [76] Y. Zhang, T. Grover, and A. Vishwanath, *Phys. Rev. Lett.* **107**, 067202 (2011).
- [77] Y. Zhang, T. Grover, A. Turner, M. Oshikawa, and A. Vishwanath, *Phys. Rev. B* **85**, 235151 (2012).
- [78] S. Yan, D. A. Huse, and S. R. White, *Science* **332**, 1173 (2011).
- [79] H.-C. Jiang, Z. Wang, and L. Balents, *Nature Physics* **8**, 902 (2012).
- [80] H.-C. Jiang, H. Yao, and L. Balents, *Phys. Rev. B* **86**, 024424 (2012).
- [81] S. Hawking, J. Maldacena, and A. Strominger, *Journal of High Energy Physics* **2001**, 001 (2001).
- [82] M. B. Hastings, *Journal of Statistical Mechanics: Theory and Experiment* **2007**, P08024 (2007).
- [83] M. M. Wolf, F. Verstraete, M. B. Hastings, and J. I. Cirac, *Phys. Rev. Lett.* **100**, 070502 (2008).
- [84] C. Holzhey, F. Larsen, and F. Wilczek, *Nuclear Physics B* **424**, 443 (1994).
- [85] P. Calabrese and J. Cardy, *Journal of Physics A: Mathematical and Theoretical* **42**, 504005 (2009).
- [86] P.-Y. Chang, J.-S. You, X. Wen, and S. Ryu, *Phys. Rev. Research* **2**, 033069 (2020).
- [87] R. Couvreur, J. L. Jacobsen, and H. Saleur, *Phys. Rev. Lett.* **119**, 040601 (2017).
- [88] L. Herviou, N. Regnault, and J. H. Bardarson, *SciPost Physics* **7**, 069 (2019).
- [89] L.-M. Chen, S. A. Chen, and P. Ye, *SciPost Phys.* **11**, 3 (2021).
- [90] N. Okuma and M. Sato, *Phys. Rev. B* **103**, 085428 (2021).
- [91] A. Bácsi and B. Dóra, *Phys. Rev. B* **103**, 085137 (2021).
- [92] R. Modak and B. P. Mandal, *Phys. Rev. A* **103**, 062416 (2021).
- [93] Y.-B. Guo, Y.-C. Yu, R.-Z. Huang, L.-P. Yang, R.-Z. Chi, H.-J. Liao, and T. Xiang, *J. Phys.: Condens. Matter* **33**, 475502 (2021).
- [94] Y.-T. Tu, Y.-C. Tzeng, and P.-Y. Chang, Rényi entropies and negative central charges in non-hermitian quantum systems (2021), arXiv:2107.13006 [cond-mat.str-el].
- [95] C. H. Lee, Exceptional boundary states and negative entanglement entropy (2020), arXiv:2011.09505 [cond-mat.quant-gas].
- [96] D. Wang, S. Xu, Y. Wang, and C. Wu, *Phys. Rev. B* **91**, 115118 (2015).
- [97] L. Li, C. H. Lee, and J. Gong, *Phys. Rev. Lett.* **124**, 250402 (2020).
- [98] D. C. Brody, *Journal of Physics A: Mathematical and Theoretical* **47**, 035305 (2013).
- [99] I. Peschel, *Journal of Physics A: Mathematical and General* **36**, L205 (2003).
- [100] S.-A. Cheong and C. L. Henley, *Phys. Rev. B* **69**, 075111 (2004).
- [101] I. Peschel and V. Eisler, *Journal of Physics A: Mathematical and Theoretical* **42**, 504003 (2009).
- [102] Z. Bai, J. Demmel, J. Dongarra, A. Ruhe, and H. van der Vorst, eds., *Templates for the solution of algebraic eigenvalue problems: A practical guide* (SIAM, Philadelphia, 2000).
- [103] H. Q. Lin, *Phys. Rev. B* **42**, 6561 (1990).
- [104] H. Lin, J. Gubernatis, H. Gould, and J. Tobochnik, *Computers in Physics* **7**, 400 (1993).
- [105] K. Kawabata, K. Shiozaki, M. Ueda, and M. Sato, *Phys. Rev. X* **9**, 041015 (2019).
- [106] P. Calabrese and J. Cardy, *Journal of Statistical Mechanics: Theory and Experiment* **2004**, P06002 (2004).
- [107] I. H. Kim, *Phys. Rev. B* **89**, 235120 (2014).
- [108] P. Fromholz, G. Magnifico, V. Vitale, T. Mendes-Santos, and M. Dalmonte, *Phys. Rev. B* **101**, 085136 (2020).
- [109] B.-T. Ye, L.-Z. Mu, and H. Fan, *Phys. Rev. B* **94**, 165167 (2016).
- [110] V. Kozii and L. Fu, Non-hermitian topological theory of finite-lifetime quasiparticles: Prediction of bulk fermi arc due to exceptional point (2017), arXiv:1708.05841 [cond-mat.mes-hall].
- [111] Y. Nagai, Y. Qi, H. Isobe, V. Kozii, and L. Fu, *Phys. Rev. Lett.* **125**, 227204 (2020).
- [112] L. Crippa, J. C. Budich, and G. Sangiovanni, *Phys. Rev. B* **104**, L121109 (2021).
- [113] J. Mitscherling and W. Metzner, *Phys. Rev. B* **104**, L201107 (2021).